An unconventional TOG domain is required for CLASP localization

Nelly Gareil, Alison Gervais, Nicolas Macaisne, Guillaume Chevreux, Julie Canman, Jessica Andreani, Julien Dumont

Report

Current Biology

An unconventional TOG domain is required for CLASP localization

Highlights

- The CLASP CTD folds as an unconventional TOG domain
- An evolutionarily conserved arginine mediates interaction with multiple CLASP partners
- Identification of novel human CLASP1 direct and indirect interactors
- The Golgin protein GOLGA4 is required for proper Golgi localization of CLASP

Authors

Nelly Gareil, Alison Gervais, Nicolas Macaisne, Guillaume Chevreux, Julie C. Canman, Jessica Andreani, Julien Dumont

Correspondence

julien.dumont@ijm.fr

In brief

Gareil and Gervais et al. demonstrate that the C-terminal domain (CTD) of CLASPs folds as an unconventional TOG domain, which has been repurposed to function as a regulatory module. The CTD mediates proper CLASP sub-cellular localization by binding to multiple partners through an evolutionarily conserved arginine.

Gareil et al., 2023, Current Biology *33*, 3522–3528
August 21, 2023
https://doi.org/10.1016/j.cub.2023.07.009

CellPress

CellPress
OPEN ACCESS

Current Biology

Report

An unconventional TOG domain is required for CLASP localization

Nelly Gareil,[1,4] Alison Gervais,[1,4] Nicolas Macaisne,[1] Guillaume Chevreux,[1] Julie C. Canman,[2] Jessica Andreani,[3] and Julien Dumont[1,5,6,*]

[1]Université Paris Cité, CNRS, Institut Jacques Monod, 75013 Paris, France
[2]Department of Pathology and Cell Biology, Columbia University, New York, NY 10032, USA
[3]Institute for Integrative Biology of the Cell (I2BC), CEA, CNRS, University of Paris Sud, Université Paris-Saclay, Gif sur Yvette, France
[4]These authors contributed equally
[5]Twitter: @ijm
[6]Lead contact
*Correspondence: julien.dumont@ijm.fr
https://doi.org/10.1016/j.cub.2023.07.009

SUMMARY

Cytoplasmic linker-associated proteins (CLASPs) form a conserved family of microtubule-associated proteins (MAPs) that maintain microtubules in a growing state by promoting rescue while suppressing catastrophe.[1] CLASP function involves an ordered array of tumor overexpressed gene (TOG) domains and binding to multiple protein partners via a conserved C-terminal domain (CTD).[2,3] In migrating cells, CLASPs concentrate at the cortex near focal adhesions as part of cortical microtubule stabilization complexes (CMSCs), via binding of their CTD to the focal adhesion protein PHLDB2/LL5β.[4,5] Cortical CLASPs also stabilize a subset of microtubules, which stimulate focal adhesion turnover and generate a polarized microtubule network toward the leading edge of migrating cells. CLASPs are also recruited to the *trans*-Golgi network (TGN) via an interaction between their CTD and the Golgin protein GCC185.[6] This allows microtubule growth toward the leading edge of migrating cells, which is required for Golgi organization, polarized intracellular transport, and cell motility.[7] In dividing cells, CLASPs are essential at kinetochores for efficient chromosome segregation and anaphase spindle integrity.[8,9] Both CENP-E and ASTRIN bind and target CLASPs to kinetochores,[10,11] although the CLASP domain required for this interaction is not known. Despite its high evolutionary conservation, the CTD remains structurally uncharacterized. Here, we find that the CTD can be structurally modeled as a TOG domain. We identify a surface-exposed and conserved arginine residue essential for CLASP CTD interaction with partner proteins. Together, our results provide a structural mechanism by which the CLASP CTD directs diverse sub-cellular localizations throughout the cell cycle.

RESULTS AND DISCUSSION

To determine the structural features important for cytoplasmic linker-associated proteins (CLASPs) to interact with other proteins, we analyzed the C-terminal domains (CTDs) of CLASPs from various species with a powerful remote homology detection algorithm. Specifically, we used HHpred against the PDB70 (clustered version of the Protein Data Bank, containing all experimentally resolved 3D structures filtered down to 70% sequence identity). Strikingly, CTD sequences were predicted, with high confidence (HHpred probability > 99%), to be homologous to structurally well-characterized tumor overexpressed gene (TOG) domains from CLASP or chTOG proteins. All CTDs were predicted to fold as a dodeca-helical domain with high conservation across species (Figures 1A and 1B).[12,13] We then performed *in silico* three-dimensional (3D) structure modeling with the AI-based AlphaFold2 algorithm.[14] The predicted architectures of all domains were very similar in the form of elongated solenoids, each composed of 12 helices, consecutively paired in 6 HEAT repeats (HRs) (Huntingtin, elongation factor 3, protein phosphatase 2A, target of rapamycin 1) (HR A to F, hereafter noted HR A to F; Figures 1C, 1D, S1A, and S1B). Overall, both the predicted secondary and tertiary structures of all analyzed CTDs conformed to those of previously characterized and crystalized TOG domains.

We assessed whether CLASP CTDs bind tubulin, like conventional TOG domains. Sequence alignment of various CLASP CTDs and comparison with human CLASP1 TOG2 revealed that the conserved residues required for tubulin interaction are lacking in the CTDs, with the notable exception of a highly conserved arginine residue in the predicted HR E (R1481 in *Hs*CLASP1α, R1458 in *Hs*CLASP2α, R970 in *Ce*CLS-2) (Figure 1B).[15] We also found no evidence that the *C. elegans* CLS-2 CTD could bind free tubulin heterodimers using a gel filtration assay (Figure S2A), which is in line with the previously reported inability of CLASP1 CTD to bind either free tubulin or microtubules.[16] Thus, the TOG-like CTD has lost the canonical tubulin-binding activity of TOG domains.

The structural similarities between different species' CTDs prompted us to test whether they could be functionally equivalent. To test this, we replaced the CLS-2 CTD with that of *Hs*CLASP1α.

CellPress
OPEN ACCESS

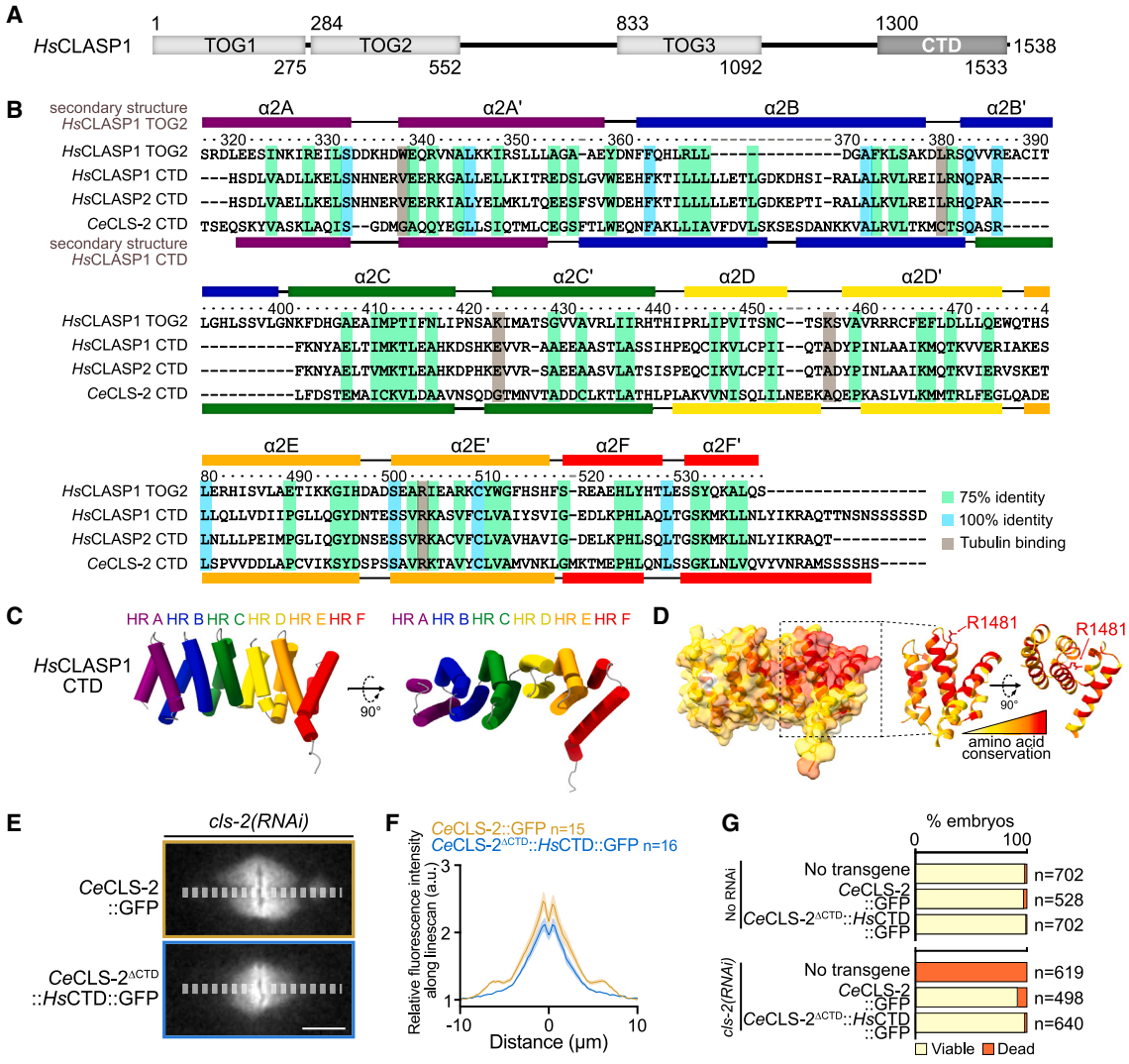

Figure 1. The CTD of CLASPs folds like a TOG domain

(A) Schematic of the *Hs*CLASP1 protein domain delimitations.

(B) Alignment and secondary structure comparison of the CTDs from *Hs*CLASP1, *Hs*CLASP2, and *Ce*CLS-2, and of the TOG2 of *Hs*CLASP1. The secondary structure of *Hs*CLASP1 TOG2 is assigned from the crystal structure and that of *Hs*CLASP1 CTD from the AlphaFold2 model.

(C and D) AlphaFold2 3D structure prediction of *Hs*CLASP1 CTD, color-coded by either (C) HEAT repeats (HRs) A–F or (D) amino acid conservation. Right: zoom on the C-terminal-conserved patch highlighting the R1481 residue. Amino acid conservation is color-coded (red, high conservation, yellow, low conservation).

(E) Still images of spindle in *C. elegans* zygotes expressing *Ce*CLS-2-GFP (orange) or *Ce*CLS-2$^{\Delta CTD}$::*Hs*CTD::GFP (blue) upon depletion of endogenous CLS-2. Scale bars, 5 μm.

(F) Quantification of mean WT *Ce*CLS-2-GFP (orange) or *Ce*CLS-2$^{\Delta CTD}$::*Hs*CTD::GFP (blue) along the mitotic spindle upon depletion of endogenous CLS-2. Error bars, SEM. Sample sizes (n metaphase plate) are indicated on the graph.

(G) Quantification of embryonic viability in the indicated conditions. Sample sizes (n embryos) are on the left of each bar plot.

See also Figure S1.

We then generated a transgenic *C. elegans* strain expressing an RNAi-resistant recoded and GFP-tagged version of this transgene (*Ce*CLS-2$^{\Delta CTD}$::*Hs*CTD::GFP). Upon RNAi-mediated depletion of endogenous CLS-2, *Ce*CLS-2$^{\Delta CTD}$::*Hs*CTD::GFP localized properly to kinetochores, although to slightly lower levels than wild-type (WT) *Ce*CLS-2-GFP. The hybrid CLASP could also sustain embryonic viability and larval development as WT GFP-tagged CLS-2 (Figures 1E–1G). Thus, the CTD of human CLASP1 can functionally replace that of *C. elegans* CLS-2, demonstrating that the CTDs are overall structurally and functionally equivalent.

We then mapped the evolutionary conservation on the surface of the CTD structural model of *Hs*CLASP1α (Figure 1D). This demonstrated that the conserved arginine residue lies in a patch of surface-exposed and conserved amino acids concentrated in the C-terminal half of the CTD, and is thus ideally positioned to mediate intermolecular interactions. To test this prediction, we mutated the conserved arginine in HR E to an alanine and we

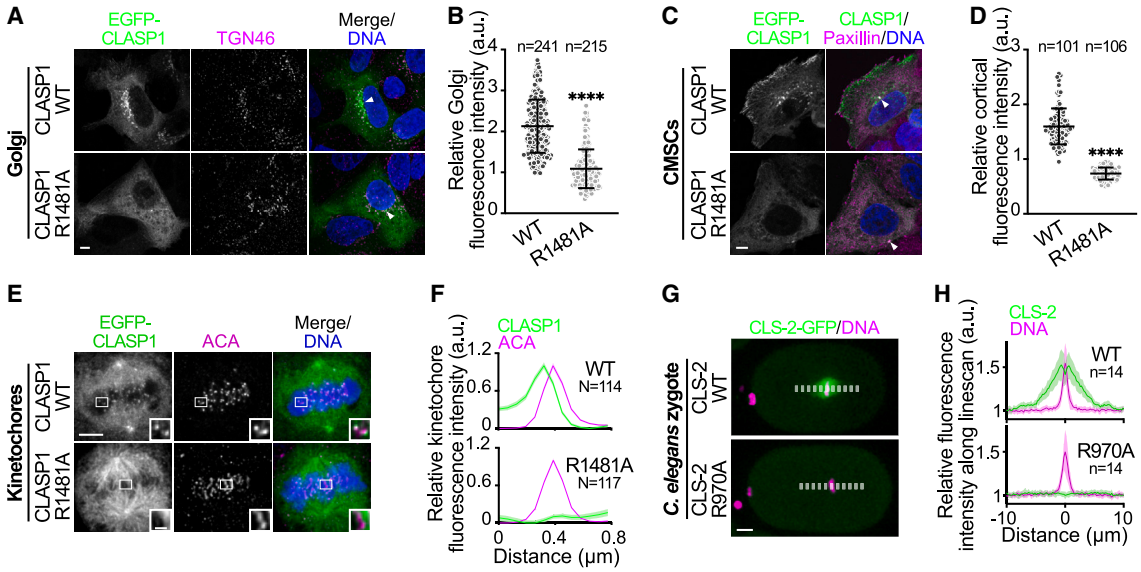

Figure 2. A conserved arginine in the CTD of CLASPs is essential for their proper sub-cellular localizations

(A–F) Immunofluorescence images of DLD-1 cells transiently expressing wild-type (WT) or R1481A EGFP-*Hs*CLASP1, and stained for (A) the *trans*-Golgi marker TGN46, (C) the focal adhesion marker paxillin, or (E) the centromeric marker ACA (bottom right: zoom on one kinetochore pair; scale bars, 1 μm). Scale bars, 5 μm. White arrowheads indicate centrosomes (localized with an anti-pericentrin antibody, not shown). Quantification of mean intensity of WT or R1481A EGFP-*Hs*CLASP1 at (B) the Golgi, (D) the cell cortex (CMSCs), and (F) kinetochores. Error bars: SD for (B) and (D), SEM for (F). Sample sizes (n areas, N kinetochores) are indicated on each graph. Unpaired t tests, $p < 0.0001$.

(G) Still images of *C. elegans* zygotes expressing WT or R970A *Ce*CLS-2-GFP and the chromosomal marker mCherry-H2B. Scale bars, 5 μm.

(H) Quantification of WT or R970A *Ce*CLS-2-GFP along the mitotic spindle. Error bars, SD. Sample sizes (n metaphase plate) are indicated on each graph.

See also Figure S2.

compared the localization of the corresponding EGFP-tagged *Hs*CLASP1α R1481A mutant and WT proteins. As expected, EGFP-*Hs*CLASP1α WT localized to centrosomes, at the cortex near focal adhesions, at the Golgi in interphase cells, and to centrosomes, spindle microtubules, and kinetochores in mitosis (Figures 2A–2F). In contrast, EGFP-*Hs*CLASP1α R1481A was absent from most interphase and mitotic sub-cellular localizations, with the notable exception of the centrosomes and along mitotic spindle microtubules. Dimerization of the mutant protein with WT CLASPs is unlikely to explain centrosome and microtubule localizations of the mutant because CLASPs in mammals do not dimerize,[17] unlike their yeast counterparts.[2,18] We made identical observations with EGFP-*Hs*CLASP2α WT and the corresponding R1458A mutant in both DLD-1 and HeLa cells (Figures S2B–S2F). Moreover, unlike WT *C. elegans* CLS-2, the R970A *Ce*CLS-2 mutant did not localize to mitotic kinetochores (Figures 2G and 2H). Thus, a conserved, putatively surface-exposed arginine residue in the CTD of CLASPs is essential for their proper sub-cellular localizations.

We also tested whether TOG domains could functionally substitute for a CLASP CTD. We previously showed that the R970A mutation in *Ce*CLS-2 abrogated the interaction with its upstream kinetochore partner proteins *Ce*HCP-1/2, which are distantly related CENP-F orthologs in mammals.[15] Here, we also found that none of the previously identified TOG domains of *Ce*CLS-2 (TOG2 and 3) interacted with the *Ce*CLS-2 binding domain (CBD) of *Ce*HCP-1, showing that although TOG domains share structural similarities with the CTD, they cannot substitute for it in the binding to partner proteins (Figure S2G).

We next determined whether mutating the surface-exposed arginine residue of human CLASPs similarly prevents their interaction with binding partners. To test this, we performed quantitative EGFP immunoprecipitations (IPs) from HEK293T cells transiently transfected with WT or the R1481A mutant human EGFP-tagged CLASP1 CTDs (Figures 3A and 3B). As expected, mass spectrometry analysis of the WT purifications recovered all known CLASP partners (Figure 3B; Data S1A). These included microtubule plus-end tracking proteins CLIP115, CLIP170, and SLAIN2, kinetochore components CENP-E and ASTRIN, the microtubule cross-linking factors SOGA1/SOGA2(MTCL1), the cell cortex proteins PHLDB2/LL5β and spectraplakin MACF1/ACF7, the centrosomal protein Ninein, and the Golgin protein GCC185. Strikingly all these interactors were significantly reduced in the R1481A mutant purifications. Comparison of CLASP1 CTD WT- and R1481A-IP proteins also recovered a number of potentially novel CLASP partners that were significantly enriched in the WT samples, including the spectraplakin DST/Dystonin and the Golgin protein GOLGA4 (Data S1A). Gene ontology analysis showed that many of the identified proteins are paralogs of known CLASP interactors (PHLDB1/3, SOGA3), known interactors of CLASP partners (MARK2 interacts with SOGA2/MTCL1, CHAMP1 is a regulator of CENP-E kinetochore localization), or localize in cellular domains where CLASPs are found (DST/Dystonin at the cell cortex, liprin α/β and CORO2B near focal adhesions, GOLGA4 at the Golgi, CENPJ/CPAP, RTTN, SASS6, CEP170, CEP250, NDE1, and BRCA2 at centrosomes). Finally, and unexpectedly, a series of proteins implicated in transcription regulation and RNA processing were associated with the CLASP CTD, including the entire five friends of

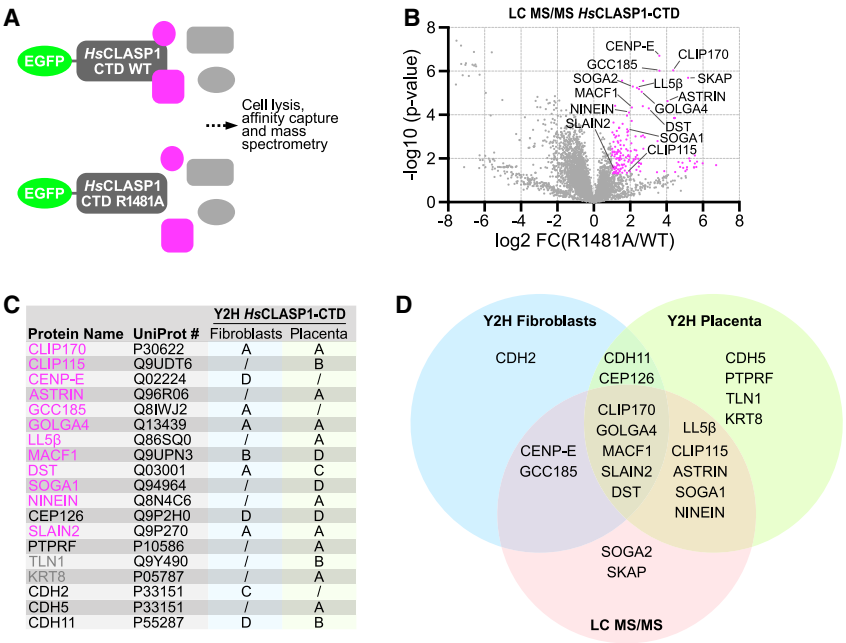

Protein Name	UniProt #	Y2H HsCLASP1-CTD Fibroblasts	Placenta
CLIP170	P30622	A	A
CLIP115	Q9UDT6	/	B
CENP-E	Q02224	D	/
ASTRIN	Q96R06	/	A
GCC185	Q8IWJ2	A	/
GOLGA4	Q13439	A	A
LL5β	Q86SQ0	/	A
MACF1	Q9UPN3	B	D
DST	Q03001	A	C
SOGA1	Q94964	/	D
NINEIN	Q8N4C6	/	A
CEP126	Q9P2H0	D	D
SLAIN2	Q9P270	A	A
PTPRF	P10586	/	A
TLN1	Q9Y490	/	B
KRT8	P05787	/	A
CDH2	P33151	C	/
CDH5	P33151	/	A
CDH11	P55287	D	B

Figure 3. Identification of *Hs*CLASP1 CTD interacting proteins

(A) Schematic of the strategy used to compare WT or R1481A *Hs*CLASP1 CTD protein partners using EGFP immunoprecipitation followed by mass-spectrometric identification.

(B) Result of LC-MS/MS analysis from four independent experiments. Volcano plot of $-\log_{10}$ p values against $\log_2$ fold change (R1481A versus WT). Proteins significantly enriched in the WT but not the R1481A mutant ($\log_2$ enrichment > 1, $p < 0.05$) are indicated in pink, with selected proteins highlighted.

(C) Result from two independent yeast-two-hybrid screens from a human fibroblast or a human placental library, respectively. The predicted biological score (PBS) of each interaction is ranked from A (very high confidence) to D (moderate confidence).[21] Proteins are highlighted as significantly enriched (pink) or not enriched (gray) in the WT compared with the R1481A mutant (identified in the proteomic analysis). Proteins not found in the proteomic analysis are displayed in black.

(D) Venn diagram displaying the overlaps between hits from the fibroblast and placenta Y2H screens, and the results from the mass spectrometry analysis (only known CLASP interactors, or proteins also identified in at least one of the Y2H screen, are included).

See also Figure S3 and Data S1.

methylated CHTOP (5FMC) complex and members of the transcription-export (TREX complex). These transcriptional regulators and RNA-processing proteins were specifically identified as WT and not R1481A mutant CTD interactors, though their physiological relevance as potential CLASP interactors is unclear.[19,20] Together, these results suggest that the conserved surface-exposed arginine residue in HR E of CLASP CTDs is essential to mediate their interaction with multiple known and potentially novel protein partners.

To detect direct interactors of the CLASP CTD, we used the CTD of human CLASP1 as a bait to conduct two yeast-two-hybrid screens from two human cDNA libraries derived from placenta or fibroblasts (Figure 3C; Data S1B and S1C). These two screens recovered several known partners of CLASPs in mammals, such as CLIP115, CLIP170, GCC185, PHLDB2/LL5β, SLAIN2, NINEIN, MACF1/ACF7, SOGA1, CENP-E, and ASTRIN. Although NINEIN, MACF1/ACF7, SOGA1, and CENP-E had previously been identified as CLASP partners, this is to our knowledge the first demonstration that these proteins can physically interact with CLASPs via the CTD. This approach also identified novel candidate CLASP-interacting proteins with a high confidence score (score of B or above), including the spectraplakin DST/Dystonin, the Golgin protein GOLGA4, the transmembrane protein tyrosine phosphatase PTPRF/LAR, the cytoskeletal proteins TLN1/Talin-1 and KRT8/Keratin-8, and some cadherins (CDH5 and 11). Importantly, several of these novel CLASP interactors were either also identified in our IP experiments (DST/Dystonin, GOLGA4, and TLN1/Talin-1) or are functionally related to known CLASP roles (PTPRF regulates focal adhesions and is a liprin-interacting protein[22–24]) (Figure 3D). This highlights their potential physiological relevance.

To validate the relevance of novel *Hs*CLASP1-CTD binding partners identified in our screens, we tested whether GOLGA4, like the Golgin protein GCC185, can recruit *Hs*CLASP1 to the *trans*-Golgi network (TGN). Indeed, we found that endogenously fluorescently tagged *Hs*CLASP1 (mNG-mAID-*Hs*CLASP1) colocalized with GOLGA4 and with the TGN integral membrane protein TGN46 (Figures S3A and S3B). To determine the importance of GOLGA4 in TGN localization of CLASP, we reduced GOLGA4 levels by 50% with small interfering RNA (siRNA) treatment. This strategy induced a proportional decrease of mNG-mAID-*Hs*CLASP1 signal at TGN46 foci, demonstrating the role of GOLGA4 in *Hs*CLASP1 localization and/or maintenance at the TGN (Figures S3B–S3D). Therefore, both GCC185 and GOLGA4, two Golgin proteins, acted in parallel and in a non-redundant manner for CLASP localization at the TGN.

The importance of the CLASP CTD in promoting sub-cellular localization likely changed through TOG-domain evolution. For example, in the budding yeast *S. cerevisiae*, localization of the CLASP ortholog Stu1 to kinetochores requires its first TOG domain (TOG1).[18] Although the molecular details of this localization are unclear, it is tempting to speculate that the Stu1 TOG1 could be functionally equivalent to CTDs and could mediate interaction with Stu1 partners essential for its localization.[25] We note, however, that the conserved arginine residue that we implicated in binding of CLASP CTDs to partner proteins is not present in the Stu1 TOG1.

In both fission and budding yeasts, a C-terminal homodimerization domain is essential for CLASP function, including for the regulation of kinetochore microtubule dynamics and binding to soluble α/β-tubulin heterodimers.[2,18,26] In contrast, mammalian CLASPs do not dimerize and seem to perform most functions as monomers *in vitro*. By analyzing the secondary structure of the domains of the *Hs*CLASP1-CTD interactors identified in our two yeast-two-hybrid screens, we noticed that most displayed coiled-coil regions. Coiled coils are usually oligomerization domains, and CLIP170, CLIP115, GCC185, CENP-E, and DST are all homodimers *in vivo*.[27–31] Each

monomer of a homodimer can potentially recruit one CLASP to a specific sub-cellular location. Thus, homodimerization of upstream interactors may have functionally replaced direct CLASP homodimerization, as observed in yeasts, as a mechanism for concentrating CLASPs at specific cell compartments.

In summary, our findings identify the CLASP CTD as an unconventional TOG domain, which has been repurposed to function as a regulatory module that mediates proper CLASP localization and potentially also function, by binding to multiple partners. In human CLASP2, the CTD has an autoinhibitory effect on TOG2 and possibly also on TOG3.[16] Relieving this autoinhibition requires binding of partner proteins to the CTD. Whether the inhibitory effect requires direct intramolecular interaction between the CTD and the rest of the protein, and whether this potential interaction involves the conserved arginine residue identified in this study, will be important to test in future studies.

STAR★METHODS

Detailed methods are provided in the online version of this paper and include the following:

- KEY RESOURCES TABLE
- RESOURCE AVAILABILITY
  - Lead contact
  - Materials availability
  - Data and code availability
- EXPERIMENTAL MODEL AND SUBJECT DETAILS
  - Cell lines and transfection
  - *C. elegans* strain maintenance
  - Transgenesis in *C. elegans*
- METHOD DETAILS
  - Secondary structure analysis
  - AlphaFold2 3D structure predictions and analysis
  - Expression constructs
  - Human cell transfection
  - RNA-mediated interference
  - Embryonic viability assay in *C. elegans*
  - Cell synchronization in mitosis
  - Protein purification
  - Protein-protein interactions by size exclusion chromatography (Gel filtration assay)
  - Immunoprecipitation and mass spectrometry
  - Samples preparation prior to LC-MS/MS analysis
  - LC-MS/MS acquisition
  - LC-MS/MS data analysis
  - Immunofluorescence
  - Microscopy
  - Yeast-two-hybrid assays
  - Generation of the mNG-mAID-*Hs*CLASP1 CRISPR DLD-1 cell line
  - Western blotting
  - Figure preparation
- QUANTIFICATION AND STATISTICAL ANALYSIS

SUPPLEMENTAL INFORMATION

Supplemental information can be found online at https://doi.org/10.1016/j.cub.2023.07.009.

ACKNOWLEDGMENTS

We thank all members of the Dumont lab for support and advice. We are grateful to Patricia Moussounda, Clarisse Picard, Téo Bitaille, and Vincent Maupu-Massamba for providing technical support, and to Benoit Palancade, Alessandro Berto, and Valérie Doye for their initial help with the yeast-two-hybrid assays. We thank Anna Akhmanova for the kind gift of pEGFP-HsCLASP1/2 plasmids and Daniele Fachinetti for providing the DLD-1 human cell lines used in this study. We thank Nicolas Joly for the gift of soluble porcine brain tubulin. Molecular graphics and analyses performed with UCSF ChimeraX, developed by the Resource for Biocomputing, Visualization, and Informatics at the University of California, San Francisco, with support from National Institutes of Health R01-GM129325 and the Office of Cyber Infrastructure and Computational Biology, National Institute of Allergy and Infectious Diseases. This work was supported by CNRS and University Paris Cité, by NIH R01GM117407 and R01GM130764 (J.C.C.), and by the European Research Council (ERC)-CoG ChromoSOMe 819179 (J.D.).

AUTHOR CONTRIBUTIONS

N.G., G.C., J.A., and J.D. conceived of the project. N.G. and A.G. performed most experiments and data analysis. N.M. performed experiments and data analysis in *C. elegans*. G.C. supervised and performed the proteomics analysis. J.A. and J.D. performed all the *in silico* modeling and analyses. N.G and J.D. designed all experiments. N.G., A.G., N.M., G.C., J.C.C., J.A., and J.D. made intellectual contributions. J.D. wrote the manuscript. J.C.C. helped with editing. N.G. and J.D. made the figures.

DECLARATION OF INTERESTS

The authors declare no competing interests.

INCLUSION AND DIVERSITY

We support inclusive, diverse, and equitable conduct of research.

Received: April 7, 2023
Revised: July 3, 2023
Accepted: July 7, 2023
Published: July 28, 2023

REFERENCES

1. Akhmanova, A., Hoogenraad, C.C., Drabek, K., Stepanova, T., Dortland, B., Verkerk, T., Vermeulen, W., Burgering, B.M., De Zeeuw, C.I., Grosveld, F., and Galjart, N. (2001). Clasps are CLIP-115 and -170 associating proteins involved in the regional regulation of microtubule dynamics in motile fibroblasts. Cell *104*, 923–935.
2. Al-Bassam, J., Kim, H., Brouhard, G., van Oijen, A., Harrison, S.C., and Chang, F. (2010). CLASP promotes microtubule rescue by recruiting tubulin dimers to the microtubule. Dev. Cell *19*, 245–258. https://doi.org/10.1016/j.devcel.2010.07.016.
3. Byrnes, A.E., and Slep, K.C. (2017). TOG-tubulin binding specificity promotes microtubule dynamics and mitotic spindle formation. J. Cell Biol. *216*, 1641–1657. https://doi.org/10.1083/jcb.201610090.
4. Lawrence, E.J., Zanic, M., and Rice, L.M. (2020). CLASPs at a glance. J. Cell Sci. *133*, jcs243097, https://doi.org/10.1242/jcs.243097.
5. Lansbergen, G., Grigoriev, I., Mimori-Kiyosue, Y., Ohtsuka, T., Higa, S., Kitajima, I., Demmers, J., Galjart, N., Houtsmuller, A.B., Grosveld, F., and Akhmanova, A. (2006). CLASPs attach microtubule plus ends to the cell cortex through a complex with LL5beta. Dev. Cell *11*, 21–32. https://doi.org/10.1016/j.devcel.2006.05.012.
6. Efimov, A., Kharitonov, A., Efimova, N., Loncarek, J., Miller, P.M., Andreyeva, N., Gleeson, P., Galjart, N., Maia, A.R.R., Mcleod, I.X., et al. (2007). Asymmetric CLASP-dependent nucleation of noncentrosomal microtubules at the trans-Golgi network. Dev. Cell *12*, 917–930. https://doi.org/10.1016/j.devcel.2007.04.002.

7. Miller, P.M., Folkmann, A.W., Maia, A.R.R., Efimova, N., Efimov, A., and Kaverina, I. (2009). Golgi-derived CLASP-dependent microtubules control Golgi organization and polarized trafficking in motile cells. Nat. Cell Biol. *11*, 1069–1080. https://doi.org/10.1038/ncb1920.

8. Pereira, A.L., Pereira, A.J., Maia, A.R.R., Drabek, K., Sayas, C.L., Hergert, P.J., Lince-Faria, M., Matos, I., Duque, C., Stepanova, T., et al. (2006). Mammalian CLASP1 and CLASP2 cooperate to ensure mitotic fidelity by regulating spindle and kinetochore function. Mol. Biol. Cell *17*, 4526–4542. https://doi.org/10.1091/mbc.E06-07-0579.

9. Maton, G., Edwards, F., Lacroix, B., Stefanutti, M., Laband, K., Lieury, T., Kim, T., Espeut, J., Canman, J.C., and Dumont, J. (2015). Kinetochore components are required for central spindle assembly. Nat. Cell Biol. *17*, 697–705. https://doi.org/10.1038/ncb3150.

10. Maffini, S., Maia, A.R.R., Manning, A.L., Maliga, Z., Pereira, A.L., Junqueira, M., Shevchenko, A., Hyman, A., iii, Y., J.R., Galjart, N., et al. (2009). Motor-independent targeting of CLASPs to kinetochores by CENP-E promotes microtubule turnover and poleward flux. Curr. Biol. *19*, 1566–1572. https://doi.org/10.1016/j.cub.2009.07.059.

11. Manning, A.L., Bakhoum, S.F., Maffini, S., Correia-Melo, C., Maiato, H., and Compton, D.A. (2010). CLASP1, astrin and Kif2b form a molecular switch that regulates kinetochore-microtubule dynamics to promote mitotic progression and fidelity. EMBO J. *29*, 3531–3543. https://doi.org/10.1038/emboj.2010.230.

12. Al-Bassam, J., Larsen, N.A., Hyman, A.A., and Harrison, S.C. (2007). Crystal structure of a TOG domain: conserved features of XMAP215/Dis1-family TOG domains and implications for tubulin binding. Structure *15*, 355–362. https://doi.org/10.1016/j.str.2007.01.012.

13. Slep, K.C., and Vale, R.D. (2007). Structural basis of microtubule plus end tracking by XMAP215, CLIP-170, and EB1. Mol. Cell *27*, 976–991. https://doi.org/10.1016/j.molcel.2007.07.023.

14. Jumper, J., Evans, R., Pritzel, A., Green, T., Figurnov, M., Ronneberger, O., Tunyasuvunakool, K., Bates, R., Žídek, A., Potapenko, A., et al. (2021). Highly accurate protein structure prediction with AlphaFold. Nature *596*, 583–589. https://doi.org/10.1038/s41586-021-03819-2.

15. Macaisne, N., Bellutti, L., Laband, K., Edwards, F., Pitayu-Nugroho, L., Gervais, A., Ganeswaran, T., Geoffroy, H., Maton, G., Canman, J.C., et al. (2023). Synergistic stabilization of microtubules by BUB-1, HCP-1, and CLS-2 controls microtubule pausing and meiotic spindle assembly. eLife *12*, e82579, https://doi.org/10.7554/eLife.82579.

16. Aher, A., Kok, M., Sharma, A., Rai, A., Olieric, N., Rodriguez-Garcia, R., Katrukha, E.A., Weinert, T., Olieric, V., Kapitein, L.C., et al. (2018). CLASP suppresses microtubule catastrophes through a single TOG domain. Dev. Cell *46*, 40–58.e8. https://doi.org/10.1016/j.devcel.2018.05.032.

17. Girão, H., Okada, N., Rodrigues, T.A., Silva, A.O., Figueiredo, A.C., Garcia, Z., Moutinho-Santos, T., Hayashi, I., Azevedo, J.E., Macedo-Ribeiro, S., and Maiato, H. (2020). CLASP2 binding to curved microtubule tips promotes flux and stabilizes kinetochore attachments. J. Cell Biol. *219*, e201905080, https://doi.org/10.1083/jcb.201905080.

18. Funk, C., Schmeiser, V., Ortiz, J., and Lechner, J. (2014). A TOGL domain specifically targets yeast CLASP to kinetochores to stabilize kinetochore microtubules. J. Cell Biol. *205*, 555–571. https://doi.org/10.1083/jcb.201310018.

19. Fanis, P., Gillemans, N., Aghajanirefah, A., Pourfarzad, F., Demmers, J., Esteghamat, F., Vadlamudi, R.K., Grosveld, F., Philipsen, S., and van Dijk, T.B. (2012). Five friends of methylated chromatin target of protein-arginine-methyltransferase[prmt]-1 (chtop), a complex linking arginine methylation to desumoylation. Mol. Cell. Proteomics *11*, 1263–1273. https://doi.org/10.1074/mcp.M112.017194.

20. Strässer, K., Masuda, S., Mason, P., Pfannstiel, J., Oppizzi, M., Rodriguez-Navarro, S., Rondón, A.G., Aguilera, A., Struhl, K., Reed, R., and Hurt, E. (2002). TREX is a conserved complex coupling transcription with messenger RNA export. Nature *417*, 304–308. https://doi.org/10.1038/nature746.

21. Formstecher, E., Aresta, S., Collura, V., Hamburger, A., Meil, A., Trehin, A., Reverdy, C., Betin, V., Maire, S., Brun, C., et al. (2005). Protein interaction mapping: a Drosophila case study. Genome Res. *15*, 376–384. https://doi.org/10.1101/gr.2659105.

22. Liang, M., Xie, X., Pan, J., Jin, G., Yu, C., and Wei, Z. (2019). Structural basis of the target-binding mode of the G protein-coupled receptor kinase-interacting protein in the regulation of focal adhesion dynamics. J. Biol. Chem. *294*, 5827–5839. https://doi.org/10.1074/jbc.RA118.006915.

23. Sarhan, A.R., Patel, T.R., Cowell, A.R., Tomlinson, M.G., Hellberg, C., Heath, J.K., Cunningham, D.L., and Hotchin, N.A. (2016). LAR protein tyrosine phosphatase regulates focal adhesions through CDK1. J. Cell Sci. *129*, 2962–2971. https://doi.org/10.1242/jcs.191379.

24. Pulido, R., Serra-Pagès, C., Tang, M., and Streuli, M. (1995). The LAR/PTP delta/PTP sigma subfamily of transmembrane protein-tyrosine-phosphatases: multiple human LAR, PTP delta, and PTP sigma isoforms are expressed in a tissue-specific manner and associate with the LAR-interacting protein LIP.1. Proc. Natl. Acad. Sci. USA *92*, 11686–11690. https://doi.org/10.1073/pnas.92.25.11686.

25. Kolenda, C., Ortiz, J., Pelzl, M., Norell, S., Schmeiser, V., and Lechner, J. (2018). Unattached kinetochores drive their own capturing by sequestering a CLASP. Nat. Commun. *9*, 886, https://doi.org/10.1038/s41467-018-03108-z.

26. Bratman, S.V., and Chang, F. (2007). Stabilization of overlapping microtubules by fission yeast CLASP. Dev. Cell *13*, 812–827. https://doi.org/10.1016/j.devcel.2007.10.015.

27. Pierre, P., Scheel, J., Rickard, J.E., and Kreis, T.E. (1992). CLIP-170 links endocytic vesicles to microtubules. Cell *70*, 887–900. https://doi.org/10.1016/0092-8674(92)90240-d.

28. Hoogenraad, C.C., Akhmanova, A., Grosveld, F., De Zeeuw, C.I., and Galjart, N. (2000). Functional analysis of CLIP-115 and its binding to microtubules. J. Cell Sci. *113*, 2285–2297. https://doi.org/10.1242/jcs.113.12.2285.

29. Luke, M.R., Houghton, F., Perugini, M.A., and Gleeson, P.A. (2005). The trans-Golgi network GRIP-domain proteins form alpha-helical homodimers. Biochem. J. *388*, 835–841. https://doi.org/10.1042/BJ20041810.

30. Kim, Y., Heuser, J.E., Waterman, C.M., and Cleveland, D.W. (2008). CENP-E combines a slow, processive motor and a flexible coiled coil to produce an essential motile kinetochore tether. J. Cell Biol. *181*, 411–419. https://doi.org/10.1083/jcb.200802189.

31. Fontao, L., Geerts, D., Kuikman, I., Koster, J., Kramer, D., and Sonnenberg, A. (2001). The interaction of plectin with actin: evidence for cross-linking of actin filaments by dimerization of the actin-binding domain of plectin. J. Cell Sci. *114*, 2065–2076. https://doi.org/10.1242/jcs.114.11.2065.

32. Laband, K., Le Borgne, R., Edwards, F., Stefanutti, M., Canman, J.C., Verbavatz, J.M., and Dumont, J. (2017). Chromosome segregation occurs by microtubule pushing in oocytes. Nat. Commun. *8*, 1499, https://doi.org/10.1038/s41467-017-01539-8.

33. Yoshino, A., Setty, S.R., Poynton, C., Whiteman, E.L., Saint-Pol, A., Burd, C.G., Johannes, L., Holzbaur, E.L., Koval, M., McCaffery, J.M., et al. (2005). tGolgin-1 (p230, golgin-245) modulates Shiga-toxin transport to the Golgi and Golgi motility towards the microtubule-organizing centre. J. Cell Sci. *118*, 2279–2293. https://doi.org/10.1242/jcs.02358.

34. Elbashir, S.M., Lendeckel, W., and Tuschl, T. (2001). RNA interference is mediated by 21- and 22-nucleotide RNAs. Genes Dev. *15*, 188–200. https://doi.org/10.1101/gad.862301.

35. Schindelin, J., Arganda-Carreras, I., Frise, E., Kaynig, V., Longair, M., Pietzsch, T., Preibisch, S., Rueden, C., Saalfeld, S., Schmid, B., et al. (2012). Fiji: an open-source platform for biological-image analysis. Nat. Methods *9*, 676–682. https://doi.org/10.1038/nmeth.2019.

36. Gabler, F., Nam, S.Z., Till, S., Mirdita, M., Steinegger, M., Söding, J., Lupas, A.N., and Alva, V. (2020). Protein sequence analysis using the MPI bioinformatics toolkit. Curr. Protoc. Bioinformatics *72*, e108, https://doi.org/10.1002/cpbi.108.

37. Mayrose, I., Graur, D., Ben-Tal, N., and Pupko, T. (2004). Comparison of site-specific rate-inference methods for protein sequences: empirical

Bayesian methods are superior. Mol. Biol. Evol. *21*, 1781–1791. https://doi.org/10.1093/molbev/msh194.

38. Remmert, M., Biegert, A., Hauser, A., and Söding, J. (2011). HHblits: lightning-fast iterative protein sequence searching by HMM-HMM alignment. Nat. Methods *9*, 173–175. https://doi.org/10.1038/nmeth.1818.
39. Katoh, K., and Standley, D.M. (2013). MAFFT multiple sequence alignment software version 7: improvements in performance and usability. Mol. Biol. Evol. *30*, 772–780. https://doi.org/10.1093/molbev/mst010.
40. Brenner, S. (1974). The genetics of *Caenorhabditis elegans*. Genetics *77*, 71–94.
41. Frøkjaer-Jensen, C., Davis, M.W., Hopkins, C.E., Newman, B.J., Thummel, J.M., Olesen, S.-P., Grunnet, M., and Jorgensen, E.M. (2008). Single-copy insertion of transgenes in Caenorhabditis elegans. Nat. Genet. *40*, 1375–1383. https://doi.org/10.1038/ng.248.
42. Leano, J.B., Rogers, S.L., and Slep, K.C. (2013). A cryptic TOG domain with a distinct architecture underlies CLASP-dependent bipolar spindle formation. Structure *21*, 939–950. https://doi.org/10.1016/j.str.2013.04.018.
43. Mirdita, M., Schütze, K., Moriwaki, Y., Heo, L., Ovchinnikov, S., and Steinegger, M. (2022). ColabFold: making protein folding accessible to all. Nat. Methods *19*, 679–682. https://doi.org/10.1038/s41592-022-01488-1.
44. Yariv, B., Yariv, E., Kessel, A., Masrati, G., Chorin, A.B., Martz, E., Mayrose, I., Pupko, T., and Ben-Tal, N. (2023). Using evolutionary data to make sense of macromolecules with a "face-lifted" ConSurf. Protein Sci. *32*, e4582, https://doi.org/10.1002/pro.4582.
45. Pettersen, E.F., Goddard, T.D., Huang, C.C., Meng, E.C., Couch, G.S., Croll, T.I., Morris, J.H., and Ferrin, T.E. (2021). UCSF ChimeraX: structure visualization for researchers, educators, and developers. Protein Sci. *30*, 70–82. https://doi.org/10.1002/pro.3943.
46. Edwards, F., Maton, G., Gareil, N., Canman, J.C., and Dumont, J. (2018). BUB-1 promotes amphitelic chromosome biorientation via multiple activities at the kinetochore. eLife *7*, e40690, https://doi.org/10.7554/eLife.40690.
47. Meier, F., Beck, S., Grassl, N., Lubeck, M., Park, M.A., Raether, O., and Mann, M. (2015). Parallel accumulation-serial fragmentation (PASEF): multiplying sequencing speed and sensitivity by synchronized scans in a trapped ion mobility device. J. Proteome Res. *14*, 5378–5387. https://doi.org/10.1021/acs.jproteome.5b00932.
48. Laband, K., Lacroix, B., Edwards, F., Canman, J.C., and Dumont, J. (2018). Live imaging of C. elegans oocytes and early embryos. Methods Cell Biol. *145*, 217–236.

STAR★METHODS

KEY RESOURCES TABLE

REAGENT or RESOURCE	SOURCE	IDENTIFIER
Antibodies		
human anti-centromere ACA	ImmunoVision	Cat#HCT-0100; RRID:AB_2744669
mouse monoclonal anti-GOLGA4	BD Biosciences	Cat#611280; RRID:AB_398808
rabbit monoclonal anti-Paxillin	Abcam	Cat#32084; RRID:AB_779033
sheep anti-TGN46	AbD Serotec	Cat#AHP500GT; RRID:AB_2203291
Alexa Fluor 488 -conjugated AffiniPure Donkey Anti-Sheep IgG (H+L)	Jackson ImmunoResearch	Cat#713-545-147; RRID:AB_2340745
Dylight 549-conjugated AffiniPure Rabbit Anti-Sheep IgG (H+L)	Jackson ImmunoResearch	Cat#313-505-003; RRID:AB_2340008
Dylight 549-conjugated AffiniPure Donkey Anti-Human IgG (H+L)	Jackson ImmunoResearch	Cat#709-506-149; RRID:AB_2340559
Dylight 649-conjugated AffiniPure Goat Anti-Rabbit IgG (H+L)	Jackson ImmunoResearch	cat#111-495-144
Donkey anti-Mouse IgG (H+L) Cross-Adsorbed Secondary Antibody, DyLight 650	Thermo Scientific	Cat#SA5-10169; RRID:AB_2556749
Peroxidase-conjugated AffiniPure Goat anti-Rabbit IgG (H+L)	Jackson ImmunoResearch	Cat#111-035-003; RRID:AB_2313567
rabbit anti-*Hs*CLASP1 primary antibody	Abcam	Cat#ab108620; RRID:AB_10864427
mouse anti-a-tubulin DM1a primary antibody	Abcam	Cat#ab7291; RRID:AB_2241126
Peroxidase-conjugated AffiniPure Goat anti-Mouse IgG (H+L)	Jackson ImmunoResearch	Cat#115-035-003; RRID:AB_10015289
GFP-Trap Magnetic Agarose beads	ChromoTek	Cat#gtma-20; RRID:AB_2631358
Bacterial and virus strains		
E. coli Strain: OP50-1	Caenorhabditis Genetic Center (CGC)	N/A
Chemicals, peptides, and recombinant proteins		
MG132	Sigma-Aldrich	Cat#C2211
Nocodazole	Sigma-Aldrich	Cat#M1404
Lipofectamine RNAiMAX	Invitrogen	Cat#13778-150
Lipofectamine 2000	Invitrogen	Cat#11668019
cOmplete, Mini, EDTA-free Protease Inhibitor Cocktail tablet	Roche	Cat#118361700001
Mowiol-DAPI	Sigma-Aldrich	Cat#81381-50G
MEGAscript T3 Transcription Kit	Invitrogen	Cat#AM1338
MEGAscript T7 Transcription Kit	Invitrogen	Cat#AM1334
MEGAclear	Invitrogen	Cat#AM1908
HiTrap TALON crude, 1 x 1 ml	Cytiva	Cat#29048565
Superdex 200 Increase 10/300 GL	Cytiva	Cat#28990944
4–20% Mini-PROTEAN TGX Stain-Free Protein Gels, 12 well, 20 μl	Biorad	Cat#4568095
3-AT	Sigma-Aldrich	Cat#A8056-10G
Critical commercial assays		
Yeast-2-hybrid screens	Hybrigenics Services	Cat#ULTImate Y2H
T7 endonuclease 1 assay	New England Biolabs	Cat#M0302
Deposited data		
Original western blot images and PDB files	Mendeley	https://doi.org/10.17632/csn2tf7c9r.1

(*Continued on next page*)

Continued

REAGENT or RESOURCE	SOURCE	IDENTIFIER
Experimental models: Cell lines		
HEK293T	gift from Matthieu Piel, Institut Curie, Paris, France	N/A
DLD-1 Flp-In T-REx expressing osTIR1	gift from Daniele Fachinetti, Institut Curie, Paris, France	N/A
HeLa	gift from Matthieu Piel, Institut Curie, Paris, France	N/A
Experimental models: Organisms/strains		
C. elegans: Strain JDU146 (ijmSi3[Pmex-5::cls-2_reencoded::gfp::tbb-2 3' UTR; Cb-unc-119 (+)]I; ijmSi31[Pmex-5::mCherry::his-11::tbb-2 3' UTR]II; unc-119(ed3)III)	Laband et al.[32]	JDU146
C. elegans: Strain JDU168 (ijmSi19[Pmex-5::cls-2reencoded_R970A::gfp::tbb-2; Cb-unc-119 (+)]I; ijmSi31[Pmex-5::mCherry::his11::tbb-2 3' UTR]II; unc-119(ed3)III)	Macaisne et al.[15]	JDU168
C. elegans: JDU788 (ijmSi159[Pmex-5::cls-2reencoded_ΔCTD:: *Hs*CLASP1_CTD::GFP::tbb-2 3'UTR; Cb-unc-119(+)]I; unc-119(ed3)III)	This study	JDU788
Oligonucleotides		
siRNA against GOLGA4: GAAUGAGGAGCAGGACAUCdTdT	Yoshino et al.[33]	N/A
siRNA against Luciferase: CGUACGCGGAAUACUUCGA	Elbashir et al.[34]	N/A
Forward oligonucleotide used to generate pLenti-Cas9-GFP-sg1*Hs*CLASP1: CACCGTTCCACTATGGAGCCTCGCA	This study	N/A
Reverse oligonucleotide used to generate pLenti-Cas9-GFP-sg1*Hs*CLASP1: AAACTGCGAGGCTCCATAGTGGAAC	This study	N/A
Forward oligonucleotide used to generate the cls-2-targeting dsRNA in *C. elegans*: TAATACGACTCACTATAGGttcaaggaaaagt tggacc	Laband et al.[32]	N/A
Reverse oligonucleotide used to generate the cls-2-targeting dsRNA in *C. elegans*: AATTAACCCTCACTAAAGGgtgcatttctga ttccacc	Laband et al.[32]	N/A
Recombinant DNA		
pEGFP-*Hs*CLASP1 (variant 1)	Gift from Anna Akhmanova lab	pJD664; NP_056097.1
pEGFP-*Hs*CLASP2 (variant 3)	Gift from Anna Akhmanova lab	pJD665; NM_001365627.1
pEGFP-*Hs*CLASP1 R1481A mutant	This study	pJD718
pEGFP-*Hs*CLASP2 R1458A mutant	This study	pJD688
pLenti-Cas9-GFP	Addgene	RRID:Addgene_86145
pProEXHTb-6xHis-*Ce*CLS-2-CTD	This study	pJD704
pP6-*Ce*CLS2-CTD	Macaisne et al.[15]	pJD844
pP6-*Ce*CLS2-CTD^{R970A}	Macaisne et al.[15]	pJD845
pP6-*Ce*CLS2-TOG2	This study	pJD848
pP6-*Ce*CLS2-TOG3	This study	pJD849
pB27-*Ce*HCP1-CLS2-BD	This study	pJD851

(*Continued on next page*)

Continued

REAGENT or RESOURCE	SOURCE	IDENTIFIER
pCFJ352-pmex-5::*Ce*CLS-2reenc(ΔCTD)::*Hs*CLASP1-CTD::GFP::3'tbb-2	This study	pJD944
Software and algorithms		
Metamorph 7	Molecular Devices	RRID: SCR_002368
Fiji	Schindelin et al.[35]	RRID: SCR_002285
Prism	GraphPad	RRID: SCR_002798
Designer	Affinity	RRID: SCR_016952
ChimeraX	UCSF	RRID: SCR_015872
AlphaFold2	Deepmind	Jumper et al.[14]
HHpred	MPI Bioinformatics Toolkit	Gabler et al.[36]
SnapGene	Dotmatics	RRID: SCR_015052
PEAKS Online X	Bioinformatics Solutions	N/A
Omics Explorer	Qlucore	N/A
Rate4Site	Tel Aviv University	Mayrose et al.[37]
HHblits	N/A	Remmert et al.[38]
MAFFT E-INS-I	N/A	Katoh et al.[39]

RESOURCE AVAILABILITY

Lead contact

Further information and requests for resources and reagents should be directed to and will be fulfilled by the lead contact, Julien Dumont (Julien.dumont@ijm.fr).

Materials availability

All unique and stable resources generated by this study are available from the lead contact without restriction.

Data and code availability

- Accession numbers are listed in the key resources table. Original western blot images and PDB files have been deposited at Mendeley Data: https://doi.org/10.17632/csn2tf7c9r.1 and are publicly available as of the date of publication. The DOI is listed in the key resources table. Microscopy data reported in this paper will be shared by the lead contact upon request.
- This paper does not report original code.
- Any additional information required to reanalyze the data reported in this paper is available from the lead contact upon request.

EXPERIMENTAL MODEL AND SUBJECT DETAILS

Cell lines and transfection

Adherent human cell lines (HeLa, HEK293T, and DLD-1) were cultured at 37°C, 5% CO_2 in DMEM + GlutaMAX medium (Gibco, #61965-026) supplemented with 1% Penicillin-Streptomycin (Gibco, #15140-122), 1% Sodium Pyruvate and 10% FBS (Gibco, #10270-106).

C. elegans strain maintenance

C. elegans strains were maintained at 23°C under standard growth conditions on NGM plates and fed with OP50-1 *E. coli*.[40]

Transgenesis in *C. elegans*

Transgenic lines used were:

JDU146 *(ijmSi3[Pmex-5::cls-2_reencoded::gfp::tbb-2 3'UTR; Cb-unc-119(+)]I; ijmSi31[Pmex-5::mCherry::his-11::tbb-2 3'UTR]II; unc-119(ed3)III)*,[32]
JDU168 *(ijmSi19[Pmex-5::cls-2reencoded_R970A::gfp::tbb-2 3′UTR; Cb-unc-119(+)]I; ijmSi31[Pmex-5::mCherry::his11::tbb-2 3' UTR]II; unc-119(ed3)III)*[15]

JDU788 *(ijmSi159[Pmex-5::cls-2reencoded_ΔCTD::HsCLASP1_CTD::GFP::tbb-2 3'UTR; Cb-unc-119(+)]I; unc-119(ed3)III)*.

The JDU788 transgenic line was obtained by Mos1-mediated Single Copy Insertion (MosSCI)[41] of the pJD944 (*pCFJ352-pmex-5::CeCLS-2reenc(ΔCTD)::HsCLASP1-CTD::GFP::3'tbb-2*) vector on Chromosome I.

All strains will be provided upon request and/or made available through the Caenorhabditis Genetics Center (CGC, https://cgc.umn.edu/).

METHOD DETAILS

Secondary structure analysis

To determine the structural features of CLASP CTDs, we analyzed *Hs*CLASP1 and *Ce*CLS-2 CTDs with a powerful remote homology detection algorithm (HHpred, https://toolkit.tuebingen.mpg.de/tools/hhpred)[36] against the PDB70 (*PDB_mmCIF70_10_Jan* database, clustered version of the Protein Data Bank containing all experimentally resolved 3D structures filtered down to 70% sequence identity). Sequence alignment of *Hs*CLASP1 TOG2, CTD, *Hs*CLASP2 CTD, and *Ce*CLS-2 CTD was done using MAFFT with standard settings in SnapGene (ver. 6.2.1). Secondary structure comparison between *Hs*CLASP1 TOG2 and CTD is based on the corresponding 3D crystal structure (4K92, α2N was removed for simplicity)[42] or on the predicted AlphaFold2 structure (*Hs*CLASP1 CTD) respectively. In both cases, intra-helix interruptions were omitted for simplicity.

AlphaFold2 3D structure predictions and analysis

All structure predictions were obtained using the ColabFold AlphaFold2_advanced notebook,[43] which is accessible at (https://github.com/sokrypton/ColabFold/), with standard parameters (multiple sequence alignment generated with MMseqs2), and the model with the highest pTMscore was selected for further analysis. All predicted 3D structures are provided as pdb supplementary files. The evolutionary conservation score of *Hs*CLASP1 CTD was calculated using the Rate4Site program[37] as a standalone (Rate4Site is the algorithm implemented in the ConSurf web server[44]). A multiple sequence alignment was generated from the full-length sequence of *Hs*CLASP1 using one iteration of HHblits[38] against the UniClust30_2018_08 database with default parameters, except for a minimum coverage of 50% with respect to the query sequence. Retrieved sequences were realigned using the MAFFT E-INS-I algorithm[39] and the top 100 sequences (closest to the query sequence) were used as the input to Rate4Site. All 3D structures were displayed using UCSF ChimeraX.[45]

Expression constructs

pEGFP-*Hs*CLASP1 (variant 1) and pEGFP-*Hs*CLASP2 (variant X15) were a kind gift from Anna Akhmanova. *Hs*CLASP1 R1481A and *Hs*CLASP2 R1458A mutants were generated by site-directed mutagenesis (QuikChange II XL Site Directed Mutagenesis Kit, Agilent Technologies, #200522).

Human cell transfection

After seeding on glass coverslips (Marienfeld, #0111520), cells were transfected with plasmids using either Lipofectamine 2000 (Invitrogen, #11668019) for HeLa and DLD-1, or calcium phosphate for HEK293T. All the cell lines used in the study were regularly tested for contamination.

RNA-mediated interference

For experiments in human DLD-1 and HeLa cells, the siRNA oligonucleotides used in this work were ordered from Dharmacon, and directed against the following target sites: GOLGA4, GAAUGAGGAGCAGGACAUCdTdT[33] (used at 240 nM for 48 hours) and Luciferase, CGUACGCGGAAUACUUCGA[34] (control siRNA, used at 240 nM for 48 hours). Transfection was performed using Lipofectamine RNAiMAX (Invitrogen, #13778-150). For experiments in *C. elegans*, the double-stranded RNA targeting *cls-2* (R107.6) was produced as described previously in Edwards et al.[46] PCR amplification was performed from total N2 cDNA using the following primers:

5'-TAATACGACTCACTATAGGttcaaggaaaagttggacc-3'

5'- AATTAACCCTCACTAAAGGgtgcatttctgattccacc-3'

Reactions were cleaned (PCR purification kit, Qiagen), and used as templates for T3 and T7 transcription reactions (MEGAscript,Invitrogen) for 5 hours at 37°C. *In vitro* transcribed RNAs were purified (MEGAclear kit, Invitrogen), then annealed at 68°C for 10 minutes, and 37°C for 30 minutes. Aliquots were snap frozen in liquid nitrogen and stored at -80°C. L4 hermaphrodite larvae were microinjected with 1500–2000 μg/μL dsRNA, singled on NGM plates and left to recover at 23°C for 48 hours before being further processed.

Embryonic viability assay in *C. elegans*

These assays were performed at 20°C. Worms were singled onto NGM plates 36 hours post-L4, upon recovery from dsRNA microinjection. Control and microinjected worms were allowed to lay eggs for 12 hours before being removed from the laying plates. For each plate, the number of dead eggs and of L1 larvae was quantified. Plates were left at 20°C for another 36 hours before counting the total number of worms reaching L4/adulthood. The proportion of viable progeny is the number of L4/adults divided by the number of dead eggs/L1.

Cell synchronization in mitosis

To enrich cells in mitosis, HeLa or DLD-1 cells were seeded on 0.01% Poly-L-Lysine (Sigma-Aldrich, P8920)-coated coverslips and incubated with 10 μM MG132 (Sigma-Aldrich, C2211) for 2 hours in complete culture medium before fixation. For immunoprecipitation and mass spectrometry analysis of CLASP partners, HEK293T cells were enriched in mitosis by incubation with 100 ng/mL Nocodazole (Sigma-Aldrich, M1404) for 17 hours in complete culture medium before lysis.

Protein purification

CLS-2-CTD was expressed in *E. coli* Rosetta2 pLysS cells using the pJD704 (pProEXHTb-6xHis-CLS-2-CTD) bacterial expression vector. Transformed bacteria were cultivated in liquid LB with ampicillin at 37°C. When the culture reached an OD600nm of ~0.75, the expression was induced with 0.5 mM IPTG at 16°C overnight.

Bacteria were harvested by centrifugation at 6000xg for 12 min. Cells were resuspended in lysis buffer (25 mM HEPES pH 7.4, 300 mM NaCl, 1 mM EDTA) supplemented with 1 mM PMSF and protease inhibitors (5 mM benzamidine and Roche - Complete EDTA-free) and lysed by sonication using a 6 mm diameter probe at 60% amplitude for 4 min (30s ON/30s OFF). The lysates were clarified by ultracentrifugation at 100,000xg for 30 min at 4°C and loaded on 1 mL HiTrap TALON Crude column (Cytiva) equilibrated with Buffer A (25 mM HEPES pH 7.4, 300 mM NaCl, 1 mM EDTA, 10% glycerol, 1 mM β-mercaptoethanol). The column was washed with 10 column volumes (CV) of buffer A followed by 10 CV of 96,7% buffer A with 3,3% buffer B (25 mM HEPES pH 7.4, 300 mM NaCl, 1 mM EDTA, 10% glycerol, 1 mM β-mercaptoethanol, 300 mM Imidazole). Elution was performed with 30 CV of a gradient from 0 to 100% buffer B. Absorbance was measured at 280 nm.

The fractions corresponding to the peak were then pooled and concentrated with Amicon Ultra-15 centrifugation units and dialysed and purified on Superdex 200 Increase 10/300GL column (Cytiva) with the dialysis buffer (25 mM HEPES pH 7.4, 150 mM NaCl, 1 mM EDTA, 10% glycerol, 1 mM β-mercaptoethanol). Fractions were analyzed by SDS-PAGE and Coomassie staining. Fractions containing pure protein were pooled, concentrated using Amicon Ultra-15 centrifugation units, frozen in liquid nitrogen and stored at -80°C.

Protein-protein interactions by size exclusion chromatography (Gel filtration assay)

To assess the interaction of the CLS-2 CTD with soluble porcine brain tubulin, a mix was prepared at equimolar concentrations of 25 μM for each protein, in an equilibration buffer (25 mM HEPES pH 7.0, 80 mM KCl, 1 mM EGTA, 1 mM MgCl2, and 5% glycerol) and incubated 2 hours at 4°C. Samples (50 μL) were loaded on a Superdex 200 Increase 10/300 GL (Cytiva) at a flow rate of 0.3 mL/minute. Protein elution from the column was followed by monitoring the absorbance at 280 nm. Peak fractions were collected and analyzed by SDS-PAGE coupled to Stain-free revelation (Biorad - Mini-PROTEAN TGX Stain-Free Gels).

Immunoprecipitation and mass spectrometry

Immunoprecipitations of EGFP-tagged *Hs*CLASP1 CTD wild-type or R1481A were performed in quadruplicate using GFP-Trap Magnetic Agarose beads (ChromoTek, gtma-20) after 24 hours of expression of the fusion proteins in HEK293T cells, according to the manufacturer's protocol. The buffers were supplemented with 1 mM PMSF, 5 mM benzamidine, and one cOmplete, Mini, EDTA-free Protease Inhibitor Cocktail tablet (Roche, 118361700001). The detergent NP-40 was substituted for IGEPAL CA-630 (Sigma-Aldrich, I8896). Briefly, cell lysates ($2.5x10^6$ cells) were incubated for 3 hours with 25 μL magnetic beads under constant wheel rotation at 4°C in Protein LoBind tubes (Eppendorf, 0030108116). After the washing steps, beads were processed for LC-MS/MS.

Samples preparation prior to LC-MS/MS analysis

Beads from pulldown experiments were incubated overnight at 37°C with 20 μL of 50 mM NH_4HCO_3 (Sigma-Aldrich) buffer containing 1 μg of sequencing-grade trypsin (Promega). The digested peptides were loaded and desalted on evotips (Evosep, Odense, Denmark) according to manufacturer's procedure before LC-MS/MS analysis.

LC-MS/MS acquisition

Samples were analyzed on a timsTOF Pro 2 mass spectrometer (Bruker Daltonics, Bremen, Germany) coupled to an Evosep one system (Evosep, Odense, Denmark) operating with the 30SPD method developed by the manufacturer. Briefly, the method is based on a 44 min gradient and a total cycle time of 48 min with a C18 analytical column (0.15 x 150 mm, 1.9 μm beads, ref EV-1106) equilibrated at 40°C and operated at a flow rate of 500 nL/min. H_2O/0.1 % MS grade formic acid (FA, ThermoFisher Scientific) was used as solvent A and ACN/ 0.1 % FA as solvent B.

The timsTOF Pro 2 was operated in PASEF mode over a 1.3 sec cycle time.[47] Mass spectra for MS and MS/MS scans were recorded between 100 and 1700 *m/z*. Ion mobility was set to 0.75–1.25 $V \cdot s/cm^2$ over a ramp time of 180 ms. Data-dependent acquisition was performed using 6 PASEF MS/MS scans per cycle with a near 100% duty cycle. Low *m/z* and singly charged ions were excluded from PASEF precursor selection by applying a filter in the *m/z* and ion mobility space. The dynamic exclusion was activated and set to 0.8 min, a target value of 16000 was specified with an intensity threshold of 1000. Collisional energy was ramped stepwise as a function of ion mobility.

LC-MS/MS data analysis

MS raw files were processed using PEAKS Online X (build 1.8, Bioinformatics Solutions). Data were searched against the Homo Sapiens SwissProt database (release 2022_04, total entry 20377). Parent mass tolerance was set to 20 ppm, with fragment mass

tolerance at 0.05 Da. Specific tryptic cleavage was selected and a maximum of 2 missed cleavages was authorized. For identification, the following post-translational modifications were included: oxidation (M), and deamidation (NQ) as variables and half of a disulfide bridge (C) as fixed. Identifications were filtered based on a 1% FDR (False Discovery Rate) threshold at both peptide and protein group levels. Label free quantification was performed using the PEAKS Online X quantification module, allowing a mass tolerance of 20 ppm, a CCS error tolerance of 0.05 and Auto Detect retention time shift tolerance for match between runs. Protein abundance was inferred using the top N peptide method and TIC was used for normalization. Multivariate statistics on proteins were performed using Qlucore Omics Explorer 3.8 (Qlucore AB, Lund, Sweden). A positive threshold value of 1 was specified to enable a $\log_2$ transformation of abundance data for normalization *i.e.*, all abundance data values below the threshold will be replaced by 1 before transformation. The transformed data were finally used for statistical analysis *i.e.*, evaluation of differentially present proteins between two groups using a Student's bilateral t-test and assuming equal variance between groups. A p-value of 0.05 was used to filter differential candidates. Results of the mass spectrometry analyses are included in Data S1A.

Immunofluorescence

HeLa and DLD-1 cells were fixed and permeabilized 24 to 72 hours after transfection, and processed for intracellular staining with suitable antibodies. Fixation was performed either 15 min in 3% PFA at room temperature (mouse monoclonal anti-GOLGA4, rabbit monoclonal anti-Paxillin and sheep anti-TGN46) or 5 min in 100% methanol at -20°C (human anti-centromere). Cell permeabilization was done in PBS-BSA-saponin (2 g/L BSA, 0.5 g/L saponin in PBS), followed by incubations with primary and secondary antibodies in the same buffer at room temperature. Cells were washed in PBS between each step. Coverslips were mounted and sealed on a glass microscopy slide in Mowiol-DAPI (Sigma-Aldrich, 81381-50G) prior to image acquisition. Primary antibodies used for immunofluorescence were: human anti-centromere (ACA, ImmunoVision, HCT-0100, 1:500), mouse monoclonal anti-GOLGA4 (BD Biosciences, 611280, 1:100), rabbit monoclonal anti-Paxillin (Abcam, 32084, 1:250), sheep anti-TGN46 (AbD Serotec, AHP500GT, 1:1000). Secondary antibodies coupled to DyLight 549, DyLight 649 or Alexa Fluor 488 (Jackson ImmunoResearch) were diluted 1:500.

Microscopy

All live and fixed acquisitions were performed on a Nikon Ti-E inverted microscope, equipped with a Yokogawa CSU-X1 spinning-disk confocal head with an emission filter wheel (Yokogawa), a laser launch with a 110 mW-405 nm, a 150 mW-488 nm, a 100 mW-561 nm, and a 110 mW-642 nm laser (Gataca Systems) using a CoolSNAP HQ2 CCD camera (Photometrics). The laser power was measured before each experiment with an Ophir VEGA Laser and energy meter. Fine stage control was performed with a PZ-2000 XYZ Piezo-driven stage (Applied Scientific Instrumentation). The microscope was controlled with Metamorph 7 software (Molecular Devices).

For *ex utero* live imaging of one-cell *C. elegans* zygotes, embryos were freed by dissecting worms on a coverslip in 6 μL meiosis medium.[48] Movies were acquired using a Nikon APO λS 60x/NA1.40 oil objective with 2x2 binning with 15 second interval, over 6 Z-planes and a step size of 2 μm. Temperature was maintained at 23°C using the CherryTemp controller system (CherryBiotech).

Fixed human cells were imaged using a Nikon APO λS 100x/NA1.45 oil objective over the entire thickness of the region of interest and a step size of 0.1 μm.

Yeast-two-hybrid assays

The two yeast-two-hybrid screenings for *Hs*CLASP1 CTD interactors were carried out by Hybrigenics Services, S.A.S. (Evry, France). The *Hs*CLASP1 CTD sequence (aa 1256 to 1538) was cloned into the pB27 vector as a C-terminal fusion with the LexA DNA-binding domain (N-LexA-*Hs*CLASP1 CTD-C fusion). This plasmid was used as a bait for the screening of two human cDNA libraries generated by random priming from a human fibroblast primary cell line or from human placenta. These libraries were cloned into the pP6 vector. The N-LexA-*Hs*CLASP1 CTD-C fusion was transformed in the YHGX13 (*Y187 ade2–101::loxP-kanMX-loxP, matα*) *S. cerevisiae* strain (MAT a), prey plasmids from the two libraries in the L40Δgal4 strain (MAT a). Upon mating of the transformed strains, 83.2 million clones and 34.8 million clones were screened from the human fibroblast and human placental libraries, respectively. 366 colonies from the human fibroblast library and 284 colonies from the human placental library were retrieved on a medium lacking tryptophan, leucine and histidine, and supplemented with 2 mM and 5 mM 3-Amino-1,2,4-Triazole (3-AT). The positive clones were PCR-amplified and sequenced at their 5′ and 3′ junctions. The corresponding interacting proteins were retrieved in the GenBank database (NCBI) by a fully automated procedure. The Predicted Biological Score (PBS) of each interaction is ranked from A (very high confidence) to D (moderate confidence).[21] Results of the yeast-two-hybrid screens are included in Data S1B (Fibroblasts) and S1C (Placenta).

The yeast-two-hybrid interaction tests between various *Ce*CLS-2 domains and the *Ce*HCP-1 CBD were performed using a similar approach. Protein domains of interest were cloned from wild type *C. elegans* (N2) cDNA. The yeast-two-hybrid assay was performed using the LexA-based system. In short, the *Ce*HCP-1 CBD was fused to the LexA binding domain in the bait pB27 plasmid. *Ce*CLS-2 TOG and CTD wild-type and R970A mutant domains were fused to the Gal4 activating domain in the prey pP6 vector. Bait-encoding plasmids were transformed in the L40Δga14 *S. cerevisiae* strain (MAT α), prey plasmids in the CG1945 strain (MAT a). Upon mating, diploid *S. cerevisae* were spotted on -Leu -Trp double-selection medium, and interactions were tested on -Leu -Trp -His medium. 5 mM of 3-Amino-1,2,4-Triazole (3-AT, Sigma-Aldrich, A8056-10G) was added to limit autoactivation by LexA::HCP-1(CBD). Image acquisitions were done on a Biorad ChemiDoc Imaging System.

Generation of the mNG-mAID-*Hs*CLASP1 CRISPR DLD-1 cell line

N-terminal tagging of endogenous *Hs*CLASP1 with mNeonGreen (mNG) and the minimal Auxin-Inducible Degradation degron (mAID) was performed in DLD-1 Flp-In T-REx expressing osTIR1 (gift from Daniele Fachinetti, Institut Curie, Paris, France) by CRISPR/Cas9 using *Streptococcus Pyogenes* Cas9 (*Sp*Cas9). Two overlapping DNA oligonucleotides (CACCGTTCCACTATGGAGCCTCGCA and AAACTGCGAGGCTCCATAGTGGAAC) were annealed and cloned at the BsmBI site of the pLenti-Cas9-GFP vector (Addgene plasmid #86145; http://n2t.net/addgene:86145; RRID:Addgene_86145) to generate pLenti-Cas9-GFP-sg1*Hs*CLASP1. Guide cutting efficiency was validated in HEK293T (48 hours after transfection) using the T7 endonuclease 1 assay (New England Biolabs, M0302). A repair template containing mNG-mAID with left and right homology arms (400 nucleotides each) was cloned in the pCR2.1 TOPO (Invitrogen TA cloning kit, 451641). The repair template was re-encoded to be sgRNA resistant, and co-transfected with the pSpCas9-GFP-sg1*Hs*CLASP1 vector using lipofectamine 2000 (Invitrogen, 11668019). 24 hours after transfection cells were fluorescently-sorted using flow cytometry to select an mNeonGreen positive pool corresponding to cells transiently-expressing the transfected plasmid with high GFP fluorescence intensity. This pool was amplified and subjected to a second sorting two weeks later for the isolation of CRIPSR clones displaying a low intensity mNeonGreen fluorescence, and corresponding to cells stably-expressing the integrated repair template after homologous recombination. Screening of clones was done by PCR from genomic DNA (Qiagen extraction kit, 158767) and clones were further validated by Sanger sequencing. Correct expression of the recombinant protein was confirmed by western blot (Figure S2D).

Western blotting

SDS-PAGE validation of the mNG-mAID-*Hs*CLASP1 CRISPR cell line was performed by migrating cell extracts on NuPAGE 3-8% Tris-Acetate gels (ThermoFisher, WG1601BX10) at 90 V using Tris-Acetate SDS running buffer (ThermoFisher, LA0041) after cell lysis in LDS sample buffer (ThermoFisher, NP0007). Protein separation was followed by liquid transfer in Towbin buffer (90 V for 80 min) on 0.45 μM nitrocellulose membrane (Amersham Protran) at 4°C. After transfer, the membrane was saturated in TBS-0.1% Tween (TBST) supplemented with 5% milk, cut in two halves between the 70 and the 100 kDa markers, before overnight incubation in the same buffer at 4°C with the rabbit anti-*Hs*CLASP1 primary antibody (Abcam, ab108620) or with the mouse anti-α-tubulin DM1α primary antibody (Abcam, ab7291) of the top and bottom halves respectively, both at 1:1000. Washing steps and incubation with secondary anti-rabbit and -mouse HRP-conjugated antibodies at 1:10000 (Jackson ImmunoResearch) were performed in TBST at room temperature for 1 hour, and followed by ECL Prime (Amersham) detection.

Figure preparation

Figures and illustrations were done in the Affinity Designer software (ver. 2.0.4).

QUANTIFICATION AND STATISTICAL ANALYSIS

For experiments performed in *C. elegans* zygotes, fluorescent intensity was measured on the frame preceding anaphase onset using ImageJ2 ver. 2.3.0 in Fiji[35] on sum projections of 6 Z-plane stacks, using 5 pixel-thick linescans along the spindle long axis centered on the zygotic metaphase plate. The background was measured using the same linescan in the cytoplasm outside the spindle area. Graphs represent the ratio of the average integrated fluorescence intensity over the background. Sample size, definition of center, dispersion and statistical tests are specified on the corresponding graphs and figure legends.

For experiments performed in human tissue cultured cells, quantifications were done using ImageJ2 ver. 2.3.0 in Fiji.[35] For the quantification of Golgi-localized CLASPs, the TGN46 staining was used to localize the Golgi. Circle ROIs (Regions Of Interest) of equal areas were drawn around the Golgi on 20 Z-plane maximum projections. Mean fluorescence intensities of TGN46, CLASP or GOLGA4 were measured within these ROIs. Fluorescence intensities of CLASP and GOLGA4 were normalized over the TGN46 signal in control and GOLGA4-depleted cells (WT CLASP1 n=241 areas, 20 cells; mutant CLASP1 n=215 areas, 20 cells; WT CLASP2 n=284 areas, 20 cells; mutant CLASP2 n=293 areas, 20 cells; siLuciferase n=147 areas, 60 cells; siGOLGA4 n=146 areas, 60 cells). For the quantification of CLASPs at the cortex, the Paxillin marker was used to localize focal adhesions. Circle ROIs of equal areas, and large enough to include both Paxillin and CLASP at CMSCs, were drawn around focal adhesions on single Z-sections. Mean fluorescence intensities of WT and mutant CLASPs were measured within these ROIs and normalized over the background signal measured outside the cells using the same size ROIs (WT CLASP1 n=101 areas, 15 cells; mutant CLASP1 n=106 areas, 15 cells; WT CLASP2 n=112 areas, 16 cells; mutant CLASP2 n=114 areas, 16 cells). Kinetochore-localized CLASPs in mitosis were quantified along centromeric linescans guided by the ACA marker on single Z-plane sections. Fluorescence intensities measured along 1-pixel thick linescans were centered on the maximum ACA fluorescence intensity. Kinetochore CLASP intensities were divided by the mean fluorescence intensity of CLASP along the spindle. Linescan analysis were normalized to set the maximum intensity equal to 1 (WT CLASP1 in HeLa N=109 kinetochores, 10 cells; mutant CLASP1 in HeLa N=93 kinetochores, 9 cells; WT CLASP2 in HeLa N=106 kinetochores, 10 cells; mutant CLASP2 in HeLa N=102 kinetochores, 10 cells; WT CLASP1 in DLD-1 N=114 kinetochores, 12 cells; mutant CLASP1 in DLD-1 N=117 kinetochores, 12 cells; WT CLASP2 in DLD-1 N=114 kinetochores, 12 cells; mutant CLASP2 in DLD-1 N=98 kinetochores, 15 cells)

Graphical representation of the mean with SEM or SD, as indicated in the corresponding figure legends, and statistical analyses using unpaired t-tests (n.s., $P \geq 0.05$ and ****, $P < 0.0001$) were performed using the GraphPad Prism software (ver. 9.5.1 (258)).